rhd instruments
flexible cell solutions

Application note

Pouch Cell Electrochemical Impedance Spectroscopy under Active Pressure and Temperature Control

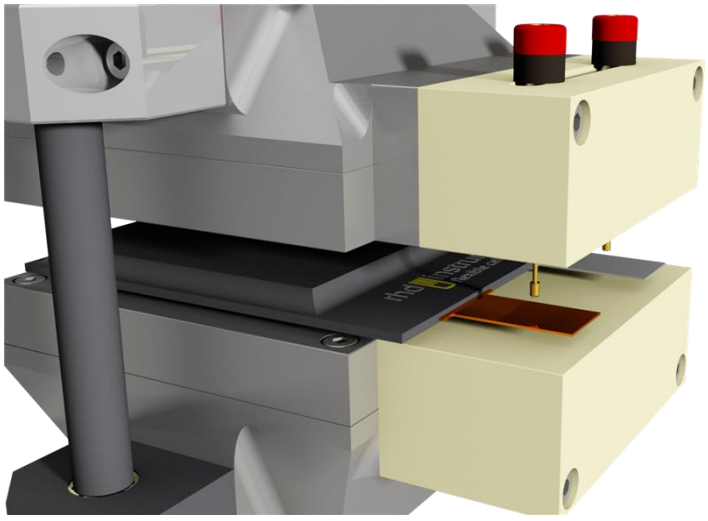

11/2022
Christoffer Karlsson, Sebastian Kranz and Benedikt Huber
rhd instruments GmbH & Co. KG

Introduction

Pouch cells constitute an important step in the battery development process, as certain performance parameters cannot be determined with small coin cell tests. It is also a popular commercial cell format with high specific energy and power. Characterization of pouch cells requires precise control of the testing conditions, such as the temperature and pressure applied to the cell stack. The temperature should be measured – and ideally also controlled – for each individual cell, since heat will be produced internally during cycling [1]. Pressure has been shown to have a large impact on the cycle life of lithium-ion battery pouch cells [1, 2, 3, 4, 5]. For lithium-metal batteries, the effect of pressure is even greater [6]. The pressure needs to be applied uniformly to the cell stack, since inhomogeneities accelerate ageing [1, 4]. Active pressure control, rather than passive control *via* springs, has also been shown to be beneficial to cycle life [5].

Electrochemical impedance spectroscopy (EIS) is one of the most powerful techniques available to characterize electrochemical systems and to distinguish between several different charge transport phenomena (*e.g.* ionic conductivity) and charge transfer reactions (*e.g.* redox reactions) occurring in a battery on various different timescales. It can also be used to monitor the internal state of the battery, and reveal the individual contributions to the total impedance (internal resistance) of the cell. Since it uses a very low alternating current, the state of charge (SOC) is not significantly changed by the measurement. By studying the effect of changing temperature, pressure and SOC, further insights into the physical quantities generating the impedance can be gained.

Experimental

For this application note, a commercial pouch cell type rechargeable lithium ion battery (ICP606168PRT, Renata AG) with a nominal capacity of 2800 mAh and a nominal average voltage of 3.7 V (**Figure 1**) was used. It had a $LiCoO_2$ (LCO) cathode and a graphite anode, with $LiPF_6$ in ethylene carbonate / ethyl methyl carbonate / diethyl carbonate (1 : 1 : 1) electrolyte and a polyethylene / polypropylene separator.

Figure 1. Lithium ion battery pouch cell tested herein.

The battery terminals (B+/B-) were connected to a protection circuit that can disconnect B- under abnormal voltage or current conditions by a MOSFET (STG8209). Under normal working

conditions, the protection circuit did not affect EIS (*i.e.* no significant difference was observed between EIS spectra when connected directly to B+/B- compared to the protected terminals P+/P-). The dimensions of the pouch cell itself (excluding protection circuitry) without any pressure applied was 63.1 mm × 58.3 mm × 5.3 mm. According to the data sheet, the cell should withstand being pressed between two flat plates at a force of 13 kN (3.5 MPa) at 100% SOC without explosion or fire.

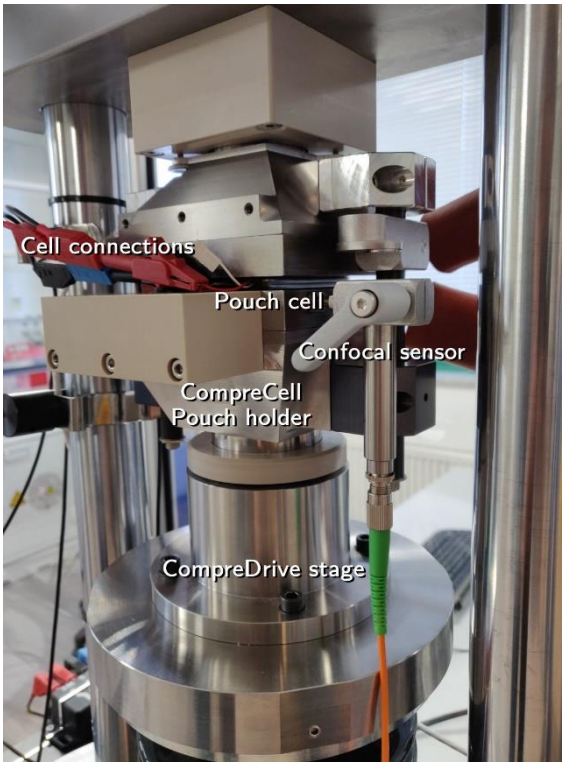

Figure 2. Experimental setup with the pouch cell mounted in the CompreCell Pouch cell holder within the CompreDrive.

The cell fixture used here was a CompreCell Pouch 10S HC cell holder mounted in a CompreDrive unit (rhd instruments GmbH & Co. KG) fitted with a confocal distance sensor add-on (Micro-Epsilon Messtechnik GmbH & Co. KG) and a 10 kN force sensor. A Huber Unistat 405 circulator (Peter Huber Kältemaschinenbau AG) with an external Pt100 sensor placed in the CompreCell Pouch cell holder was used for temperature control. The software CompreDriveControl 1.13 (rhd instruments GmbH & Co. KG) with the rhd MicroEpsilon Confocal Server plugin (rhd instruments GmbH & Co. KG) was used for data logging and control of the CompreDrive and circulator. The pouch cell P+/P- terminals were contacted by alligator clips, rather than by the standard CompreCell Pouch pins, which are used for flat tabs (see figure on title page). The experimental setup with the pouch cell in place can be seen in **Figure 2**. After the CompreDrive stage was approached (8.2 kPa applied stack pressure for this size of pouch cell), the distance value of the confocal sensor was tared according to the *ex situ* measured cell thickness.

A Metrohm Autolab PGSTAT302N equipped with a FRA32 module and controlled through the NOVA 2.1.5 software was used for all electrochemical measurements. The tests were automated through the CompreDriveRemote 1.13 (rhd instruments GmbH & Co. KG) functionality, allowing automated control of the CompreDrive pressure and temperature from a NOVA procedure. EIS was performed in galvanostatic mode with an rms amplitude of C/100 (28 mA) in a frequency range of 100 kHz to 1 mHz (10 points per decade). The recorded impedance data were evaluated by

equivalent circuit fitting using the impedance data analysis software RelaxIS 3 (rhd instruments GmbH & Co. KG).

Initially, a temperature of 25 °C and a pressure of 0.5 MPa was applied to the cell, and three C/2 (1.4 A) charge/discharge cycles were performed to verify the cell capacity. (Details on the charge/discharge conditions are described elsewhere [7].) The cell was then charged to 50 % SOC, and EIS spectra measured at 5, 25, and 45 °C, and 0.5, 1.0, 1.5, and 2.0 MPa. The cell was charged at 25 °C and 0.5 MPa, and on the subsequent discharge cycle, EIS spectra were recorded at varying SOC (10 % SOC steps), with a 1 h resting time before starting each EIS measurement. The cell was then subjected to cycling at different temperatures and pressures, which is described in a separate application note [7]. Throughout all testing, the thickness of the pouch cell was monitored *in operando* to ensure stable conditions during the EIS measurements [7].

WARNING! Lithium-ion batteries are flammable! Thermal runaway can be caused by applying improper voltage, current, temperature or pressure to the cell!

Results

EIS spectra collected at varying SOC and temperature can be seen in **Figure 3**. At high frequencies (>1 kHz), the inductance (I) of cables and current collectors is visible in the spectra as a positive Z''. An increase in Z' with frequency in the inductive region indicates some energy loss (R_{loss}) which might arise from eddy currents in the current collector sheets [8]. The intercept with the Z' axis around 105 mΩ at 1 kHz roughly approximates the series resistance (R_{series}) of the cell, but should not be used directly due to the substantial inductance. At intermediate frequencies, a flattened semicircle is observed in the Nyquist plot, originating from overlapping charge transfer (R_{ct}) processes with simultaneous double layer charging (C_{dl}) occurring across the various interfaces in the battery cell, such as the current collector | active material interfaces, and the active material | electrolyte interfaces. At low frequencies (below about 1 Hz) increasing impedance is observed arising from solid state diffusion in the active material particles. It is however not a simple behaviour with a constant phase angle, but also exhibits an intermediate stage with a lower phase angle. This indicates that several different diffusion processes are occurring, a feature which is sometimes observed for LCO based batteries [9]. It can in principle arise from several causes, such as the bimodal particle size distribution of the cathode active material [9], ionic diffusion through the separator [10], or non-cylindrical or fractal active material pores [11]. The two-stage diffusion behaviour was more pronounced at high and low SOC than at intermediate SOC. For the temperature and pressure dependent spectra (recorded at 50 %

SOC), the diffusion part of the spectra was therefore more or less linear (**Figure 3c**).

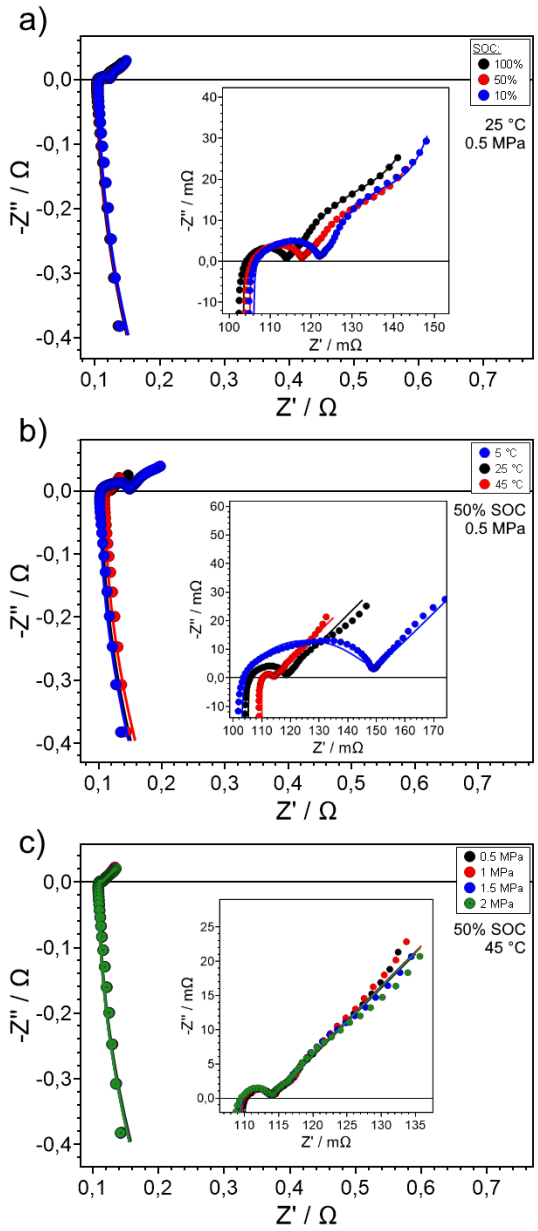

Figure 3. Nyquist plots of EIS spectra at varying a) SOC (25 °C, 0.5 MPa), b) temperature (0.5 MPa, 50 % SOC) and c) pressure (45 °C, 50 % SOC). Lines indicate fits to the equivalent circuits in Figure 4.

With decreasing SOC, the EIS spectra shifted to the right and the width of the semicircle increased (**Figure 3a**). The temperature dramatically affected the impedance of the cell, shifting the high-frequency impedance to larger values with higher temperature, as well as decreasing width of the semicircle. Thus, the impedance (on a time scale longer than 0.1 s) decreased with temperature, in accordance with the overpotential observed during cycling [7]. At 5 °C (blue curve in **Figure 3b**) the semicircle started to separate into two distinct semicircles, as the difference in activation energies between charge transfer processes lead to a separation in time scales. Meanwhile, the pressure had little visible impact on the EIS spectra (**Figure 3c**).

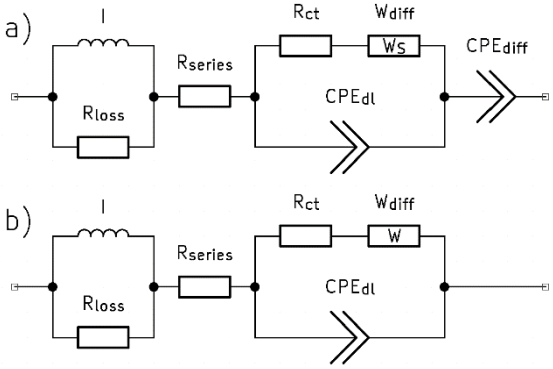

Figure 4. Equivalent circuits used for fitting of a) SOC dependent and b) temperature and pressure dependent EIS data, respectively.

According to the EIS spectrum features described above, the equivalent circuits shown in **Figure 4** were fitted to the spectra. A constant phase element (CPE) was used for the double layer capacitance, rather than an ideal capacitor, to account for the flattened shape of the semicircle. Spectra at 5 °C could be better fitted with an extra R_{ct}/CPE_{dl} element to account for the separation of the semicircle, but for comparison purposes the same circuit was used for all temperatures (**Figure 4b**).

Since the SOC dependent data exhibited a two-stage diffusion process, a finite diffusion Warburg short element in addition to a CPE element was used (**Figure 4a**). In the temperature and pressure dependent data, on the other hand, the diffusion part was simply fitted with an infinite diffusion Warburg element (**Figure 4b**) since the two-stage process was not very distinct.

As expected from the qualitative analysis of the spectra described above, R_{series} and R_{ct} both decreased with SOC (**Figure 5**). The decrease in R_{series} was minor (from 106 to 103 mΩ) and probably related to the change in pore structure of the active materials. R_{ct} decreased substantially (from 16 to 10 mΩ) with SOC, relating to the ease of lithium insertion/deinsertion in the cathode, and intercalation/deintercalation in the anode.

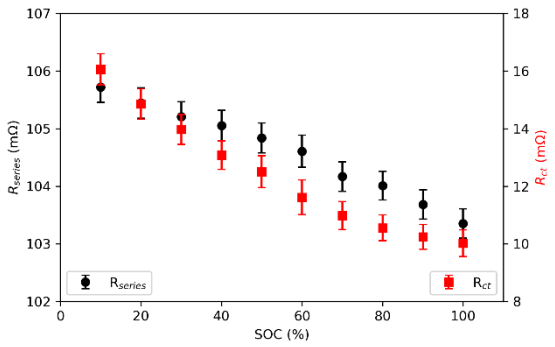

Figure 5. Series resistance (black circles, left y-axis) and charge transfer resistance (red squares, right y-axis) *vs* SOC (25 °C, 0.5 MPa). *N.B.* Error bars indicate the fit errors, not experimental errors.

The series resistance of the cell increased with temperature, indicating that the main contributor to this resistance is the electronic resistance, and not the ionic resistance of the electrolyte (**Figure 6**). The charge transfer resistance, however, decreased with temperature according to the Arrhenius equation:

$$\frac{1}{R_{ct}} = Ae^{-\frac{E_a}{k_B T}}$$

where A is a preexponential factor corresponding to the reciprocal of R_{ct} at infinite temperature, E_a is the activation energy, and k_B is the Boltzmann constant. Fitting the R_{ct} values to the Arrhenius equation in RelaxIS 3 yielded the pressure dependent E_a shown in the inset in **Figure 6** ($r^2 > 0.9999$ for all pressures, but note that only three data points were used for each fit here). Thus, even though the pressure did not have a large impact on the resistances measured by EIS, its effect on the activation energy could be discerned.

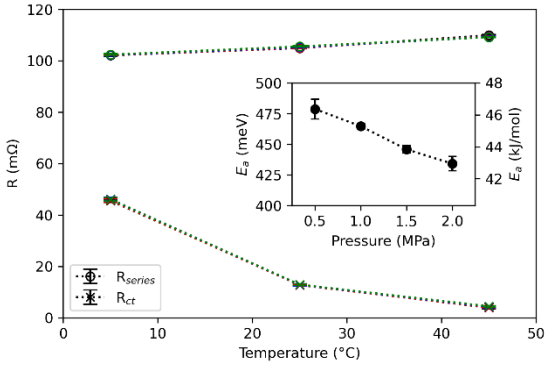

Figure 6. Series resistance (circles) and charge transfer resistance (crosses) *vs* temperature at 0.5 (black), 1.0 (red), 1.5 (blue) and 2.0 (green) MPa (50% SOC). The inset shows the charge transfer activation energy *vs* pressure. *N.B.* Error bars indicate the fit errors, not experimental errors.

E_a was in the range 430 – 480 meV, decreasing with the applied pressure. This is at the lower end of the range of

commonly reported E_a values for this cell chemistry (*e.g.* 550 – 740 meV for graphite [12, 13, 14] and 550 – 620 meV for LCO [13, 14]), meaning that it is slightly less sensitive to operating at lower temperatures. The decrease in E_a with pressure could be due to improved contacts between the interfaces.

Summary

The impedance response of a commercial lithium-ion battery pouch cell was investigated under active temperature and pressure control. The SOC and temperature had a large impact on the series resistance, charge transfer resistance and diffusion behaviour of the cell. A pressure-dependent activation energy was obtained for the charge transfer resistance. The activation energy decreased from 0.48 eV at 0.5 MPa to 0.43 eV at 2.0 MPa, possibly as an effect of improved interfacial contact between the different layers in the pouch cell. The CompreDrive system with the CompreCell Pouch cell holder allows for active pressure control and applies uniaxial and homogeneous pressure to the cell stack, which is necessary for high reproducibility.

Literature

[1] T. Deich, S. L. Hahn, S. Both, K. P. Birke and A. Bund, "Validation of an actively-controlled pneumatic press to simulate automotive module stiffness for mechanically representative lithium-ion cell aging," *Journal of Energy Storage*, vol. 28, p. 101192, 2020.

[2] G. Berckmans, L. D. Sutter, M. Marinaro, J. Smekens, J. Jaguemont, M. Wohlfahrt-Mehrens, J. v. Mierlo and N. Omar, "Analysis of the effect of applying external mechanical pressure on next generation silicon alloy lithium-ion cells," *Electrochimica Acta*, vol. 306, pp. 387-395, 2019.

[3] A. S. Mussa, M. Klett, G. Lindbergh and R. W. Lindström, "Effects of external pressure on the performance and ageing of single-layer lithium-ion pouch cells," *Journal of Power Sources*, vol. 385, pp. 18-26, 2018.

[4] V. Müller, R.-G. Scurtu, K. Richter, T. Waldmann, M. Memm, M. A. Danzer and M. Wohlfahrt-Mehrens, "Effects of Mechanical Compression on the Aging and the Expansion Behavior of Si/C-Composite|NMC811 in Different Lithium-Ion Battery Cell Formats," *Journal of The Electrochemical Society*, vol. 166, no. 15, pp. A3796-A3805, 2019.

[5] M. Wünsch, J. Kaufman and D. U. Sauer, "Investigation of the influence of different bracing of automotive pouch cells on cyclic liefetime and impedance spectra," *Journal of*

Energy Storage, vol. 21, pp. 149-155, 2019.

[6] C. Fang, B. Lu, G. Pawar, M. Zhang, D. Cheng, S. Chen, M. Ceja, J.-M. Doux, H. Musrock, M. Cai, B. Liaw and Y. S. Meng, "Pressure-tailored lithium deposition and dissolution in lithium metal batteries," *Nature Energy,* vol. 6, no. 10, pp. 987-994, 2021.

[7] C. Karlsson, S. Kranz and B. Huber, "Application Note: In Operando Pouch Cell Thickness Monitoring during Cycling under Controlled Temperature and Pressure," November 2022. [Online]. Available: https://rhd-instruments.de/download/appnotes/application-note_CompreDrive_Pouch_Cell_Thickness.pdf.

[8] "Application note: Determining Through-Plane Membrane Conductivity using Four-Electrode EIS," August 2022. [Online]. Available: https://rhd-instruments.de/download/appnotes/application-note_TCE%20Cell%20One_Four_electrode_membrane_conductivity.pdf.

[9] T. Osaka, D. Mukoyama and H. Nara, "Development of Diagnostic Process for Commercially Available Batteries, Especially Lithium Ion Battery," *Journal of The Electrochemical Society,* vol. 162, no. 14, pp. A2529-A2537, 2015.

[10] J. Moškon, J. Žuntar, S. D. Talian, R. Dominko and M. Gaberšček, "A Powerful Transmission Line Model for Analysis of Impedance of Insertion Battery Cells: A Case Study on the NMC-Li System," *Journal of The Electrochemical Society,* vol. 167, p. 140539, 2020.

[11] S. J. Cooper, A. Bertei, D. P. Finegan and N. P. Brandon, "Simulated impedance of diffusion in porous media," *Electrochimica Acta,* vol. 251, pp. 681-689, 2017.

[12] T. R. Jow, S. A. Delp, J. L. Allen, J.-P. Jones and M. C. Smart, "Factors Limiting Li+ Charge Transfer Kinetics in Li-Ion Batteries," *Journal of The Electrochemical Society,* vol. 165, no. 2, pp. A361-A367, 2018.

[13] A. Tomaszewska, Z. Chu, X. Feng, S. O'Kane, X. Liu, J. Chen, C. Ji, E. Endler, R. Li, L. Liu, Y. Li, S. Zheng, S. Vetterlein, M. Gao, J. Du, M. Parkes, M. Ouyang, M. Marinescu, G. Offer and B. Wu, "Lithium-ion battery fast charging: A review," *eTransportation,* vol. 1, p. 100011, 2019.

[14] Z. Ogumi, "Interfacial Reactions of Lithium-ion Batteries," *Electrochemistry,* vol. 78, no. 5, pp. 319-324, 2010.